

Accretion and star formation in ‘radio-quiet’ quasars

Sarah V. White (SVW)^{1,2,3}, Matt J. Jarvis^{3,4}, Eleni Kalfountzou^{5,6},
Martin J. Hardcastle⁶, Aprajita Verma³, José M. Cao Orjales⁶
and Jason Stevens⁶

¹South African Radio Astronomy Observatory (SARAO), 2 Fir Street, Observatory, Cape Town, 7925, South Africa. ²Department of Physics and Electronics, Rhodes University, PO Box 94, Grahamstown, 6140, South Africa. ³Astrophysics, University of Oxford, Denys Wilkinson Building, Keble Road, Oxford, OX1 3RH, UK
email: sarahwhite.astro@gmail.com

⁴Department of Physics, University of the Western Cape, Bellville 7535, South Africa

⁵European Space Astronomy Centre (ESAC), Villanueva de la Cañada, E-28692 Madrid, Spain

⁶Centre for Astrophysics Research, School of Physics, Astronomy and Mathematics, University of Hertfordshire, Hatfield, Herts, AL10 9AB, UK

Abstract. Radio observations allow us to identify a wide range of active galactic nuclei (AGN), which play a significant role in the evolution of galaxies. Amongst AGN at low radio-luminosities is the ‘radio-quiet’ quasar (RQQ) population, but how they contribute to the total radio emission is under debate, with previous studies arguing that it is predominantly through star formation. In this talk, SVW summarised the results of recent papers on RQQs, including the use of far-infrared data to disentangle the radio emission from the AGN and that from star formation. This provides evidence that black-hole accretion, instead, dominates the radio emission in RQQs. In addition, we find that this accretion-related emission is correlated with the optical luminosity of the quasar, whilst a weaker luminosity-dependence is evident for the radio emission connected with star formation. What remains unclear is the process by which this accretion-related emission is produced. Understanding this for RQQs will then allow us to investigate how this type of AGN influences its surroundings. Such studies have important implications for modelling AGN feedback, and for determining the accretion and star-formation histories of the Universe.

Keywords. galaxies: active – galaxies: statistics – galaxies: evolution – galaxies: high-redshift – quasars: general – radio continuum: galaxies

1. Radio emission from ‘radio-quiet’ quasars

Star formation and black-hole accretion are the key processes that govern how galaxies evolve. Since both processes produce radio emission, deep radio surveys enable complete selection of galaxies out to high redshift, unaffected by dust obscuration (unlike optical surveys) or Compton-thick absorption (unlike X-ray surveys). However, as is the case at other wavelengths, the contributions of star formation and the active galactic nucleus (AGN) towards the total emission need to be disentangled. The techniques we use to do this will prove particularly important for science with the Square Kilometre Array (SKA) and its precursor/pathfinder telescopes (e.g. McAlpine et al., 2015; Jarvis et al., 2015). As we probe to lower radio flux-densities (< 1 mJy), a flattening of the source counts implies that we are going from an AGN dominated regime to a star-formation dominated regime (Condon et al., 2012). However, it is not only star-forming galaxies that are detected below 1 mJy. We also uncover the population of radio-quiet quasars [RQQs; see predictions by Wilman et al. (2008)], which are a subset of AGN that produce relatively low levels of radio emission when compared to their ‘radio-loud’ counterparts.

Table 1. The accretion-related contribution to the radio luminosity, across our sample of RQQs. An object with $L_{1.5 \text{ GHz, acc}}/L_{1.5 \text{ GHz}} > 0.5$ is described as being ‘AGN-dominated’. ‘Summed radio luminosity’ refers to the summation of the total radio luminosity for each object ($\Sigma L_{1.5 \text{ GHz}}$), and the ‘fraction that is accretion-related’ is given by $\Sigma L_{1.5 \text{ GHz, acc}}/\Sigma L_{1.5 \text{ GHz}}$. ‘Upper’ and ‘lower’ limits refer to the fraction of the radio emission that is related to accretion, taking into account cases where the object is undetected (i.e. $< 2\sigma$) in the radio and/or the FIR.

Description of objects used (and the $L_{1.5 \text{ GHz, acc}}$ values considered)	No. of objects	Fraction that are AGN-dominated	Summed radio luminosity (W Hz^{-1})	Fraction of summed luminosity that is accretion-related
Whole sample	70	0.80	3.82×10^{25}	0.74
Whole sample (lower limits)	70	≥ 0.47	$\leq 5.28 \times 10^{25}$	≥ 0.60
Whole sample (upper limits)	70	≤ 0.89	$\leq 5.28 \times 10^{25}$	≤ 0.83
Radio-detected, FIR-detected	26	0.92	3.07×10^{25}	0.80

The current assumption is that star formation is responsible for the radio emission from RQQs, with Kimball et al. (2011) and Condon et al. (2013) favouring this interpretation. However, these studies use only radio and optical data for their analyses. For our work, we take a step further by also using far-infrared (FIR) data from the *Herschel Space Observatory*, reduced and presented by Kalfountzou et al. (2017). This allows us to *quantify* the level of star formation within our sample of 70 RQQs, by combining the derived far-infrared luminosities with the far-infrared to radio correlation (FIRC). This very tight relation is observed for star-forming galaxies, and arises due to star formation being associated with both dust (producing the FIR emission) and supernova remnants (producing radio emission).

2. Disentangling black-hole accretion from star formation

Like the quasars used by Kimball et al. (2011) and Condon et al. (2013), our sample is selected from the Sloan Digital Sky Survey (SDSS), but we restrict the redshift range to $0.9 < z < 1.1$ in order to minimise any possible evolutionary effects. The radio data we use is in the form of targeted observations using the Karl G. Jansky Very Large Array, enabling us to reach a sensitivity of $\sim 30 \mu\text{Jy}$ in 25 minutes of integration time per source [PI: Jarvis; White et al. (2017)]. When analysed in conjunction with FIR data, we find that for the majority of our RQQs, there is a significant amount of radio emission that cannot be explained by star formation alone. This is illustrated by the RQQs lying to the right of the FIRC in Fig. 1, having ‘excess’ radio emission. The excess emission must be due to another process – that being black-hole accretion – and so we use the offsets from the FIRC to calculate the accretion-related radio luminosity. As shown by the numbers in Table 1, this accretion component is dominating the total radio emission from our RQQs, in support of previous work by White et al. (2015) and going against the assumption that star formation dominates. Our fractions may even be underestimates, given a study by Wong et al. (2016) that shows a sample of hard X-ray selected AGN lying on the FIRC, mimicking the properties of star-forming galaxies.

Another aspect of our sample is that it has been downselected in order to enforce a uniform distribution in absolute i -band magnitude, spanning a factor of ~ 100 in optical luminosity. This allows us to explore whether there is any trend in the star-formation-related radio luminosity, or the accretion-related radio luminosity, with the optical luminosity of the quasar. White et al. (2017) find a stronger statistical correlation for the latter combination, which is as expected since the accretion disc of a quasar produces

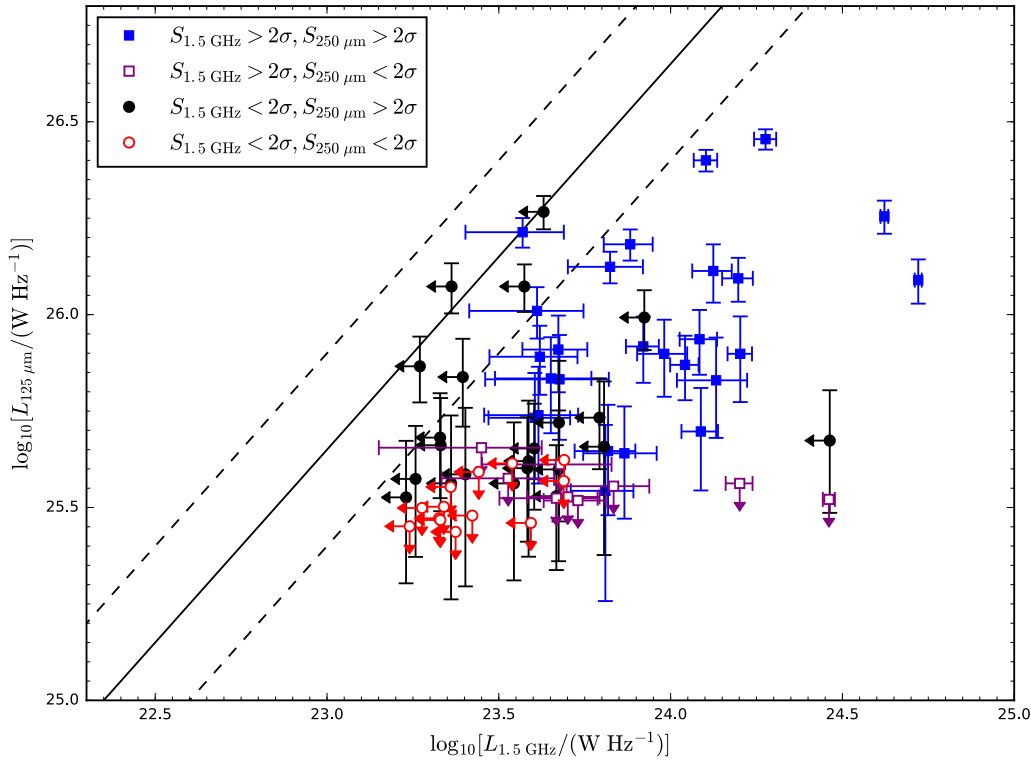


Figure 1. The FIR luminosity at rest-frame $125\ \mu\text{m}$, $L_{125\ \mu\text{m}}$, versus the radio luminosity, $L_{1.5\ \text{GHz}}$. Squares correspond to objects detected in the radio above 2σ , and circles are those below this detection threshold. Note that objects with $\log_{10}[L_{125\ \mu\text{m}}] \lesssim 25.6$ are below 2σ at $250\ \mu\text{m}$ (unfilled symbols). Arrows represent $2\text{-}\sigma$ upper limits in $L_{1.5\ \text{GHz}}$ or $L_{125\ \mu\text{m}}$, for quasars undetected at the $2\text{-}\sigma$ level in the radio (horizontal arrows) or the $250\ \mu\text{m}$ photometry (vertical arrows), respectively. The dashed lines are the lower and upper bounds on q_{125} (2.4 and 2.9, respectively), where $q_{125} = \log_{10}[L_{125\ \mu\text{m}}/L_{1.5\ \text{GHz}}]$. The solid line corresponds to the midpoint value, $q_{125} = 2.65$, and represents the FIRC (where star-forming galaxies are expected to lie). *Figure reproduced from White et al. (2017).*

thermal emission that dominates the i band. We therefore have further evidence that this component of the radio emission truly is connected with the AGN. However, a lot of scatter is still seen between the accretion-related radio luminosity and the absolute i -band magnitude (Fig. 2), which could be due to variations in magnetic-field strength, environmental density, or the differing timescales over which the radio emission and optical emission are produced.

3. What accretion-related mechanism is present?

We have concluded that the AGN is dominating the total radio emission from RQQs, but the exact mechanism involved requires further investigation. It is possible that radio jets (typically associated with ‘radio-loud’ quasars) are being launched (e.g. Hartley et al., 2019) but they are too small to be resolved in our radio images. Supporting this, earlier in the Symposium we were shown images of small jets in ‘radio-silent’ Seyfert galaxies (Lähteenmäki et al., 2018), which are believed to be low-redshift analogues of quasars. Another suggestion, regarding the origin of the AGN-related radio emission, is

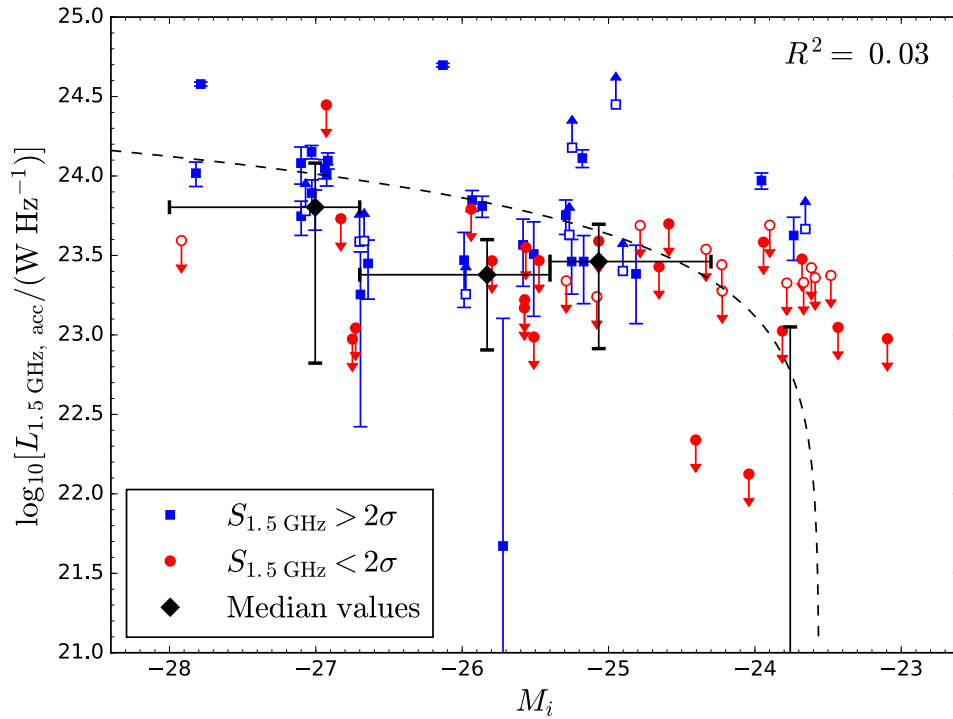


Figure 2. The accretion luminosity, $L_{1.5 \text{ GHz, acc}}$ against the absolute i -band magnitude, M_i . Blue squares correspond to objects detected in the radio above 2σ , and red circles are those below this detection threshold. Unfilled symbols correspond to the FIR data being below 2σ . Arrows indicate whether the value of $L_{1.5 \text{ GHz, acc}}$ is either an upper or lower limit (at 2σ), dependent on whether the object is undetected in both the radio and the FIR, or undetected in the FIR alone. The line of best-fit is given by $L_{1.5 \text{ GHz, acc}} = (-2.99 \pm 0.84) \times 10^{23} M_i - (7.05 \pm 2.11) \times 10^{24}$, and the associated coefficient of determination is shown in the top right-hand corner. (Uncertainties in $L_{1.5 \text{ GHz, SF}}$ and $L_{1.5 \text{ GHz, acc}}$ are used for this fit.) The dashed line is the result of converting this best-fit line into log-linear space. Overplotted are the median luminosities (black diamonds), derived using all objects, binned in M_i . The horizontal error-bars indicate the ranges of the M_i bins, and uncertainties on the median radio-luminosities are given by the vertical error-bars. Note that the values of the luminosities, even if negative, are used for the linear regression analysis and the calculation of the median luminosities, rather than the limit values. *Figure reproduced from White et al. (2017).*

that it is associated with an X-ray corona close to the accretion disc (Laor & Behar, 2008), with similar magnetic connection events as seen for coronally-active stars.

Alternatively, the winds associated with the accretion disc may be impacting upon the surrounding medium and creating shock fronts, which in turn accelerate electrons and generate radio emission. Hwang et al. (2018) provide evidence for this explanation, by looking at the radio luminosity of quasars against the equivalent width of the [OIII] emission line. This quantity acts as a proxy for the quasar’s outflow velocity, and they find that an ‘extreme’ sample of high-redshift quasars appears to lie on the same correlation observed for their previous sample of low-redshift quasars. However, they cannot completely rule out the possibility of compact jets being present, as these could give rise to the same kinematics as quasar winds. Indeed, later during the Symposium, Jarvis et al. (2019) presented results for *jetted* RQQs lying on the relation by Hwang et al. (2018).

4. Implications and future work

Understanding the origin of the radio emission in radio-quiet AGN is important if we wish to: (i) use faint sources to probe the star-formation history of the Universe, or how accretion activity has evolved; (ii) uncover why some quasars exhibit powerful radio-jets whilst the majority do not; and (iii) see whether we need to consider feedback from radio-quiet AGN as well as from radio-loud AGN. This is particularly important for modelling galaxy evolution. For example, Mancuso et al. (2017) have used our ‘disentangled’ radio luminosities to test their models of star formation and accretion in the radio band, for which they consider in-situ co-evolution of the two processes. They find that our RQQs lie on the average relationship between the accretion radio-luminosity and the star-formation radio-luminosity, averaged across *all* galaxies (since radio data offer complete selection).

Most recently, Malefahlo et al. (submitted) present radio luminosity functions (RLFs), over multiple redshift ranges, for optically-selected quasars identified in SDSS. For this they use a Bayesian stacking analysis to probe below the 1-mJy flux-limit of the FIRST survey (Becker et al., 1995). White et al. will test the radio-quiet distribution of these RLFs using optical spectroscopy from the Southern African Large Telescope (PI: White) and deep radio data that has been obtained as part of the MIGHTEE survey (Jarvis et al., 2016). Following this is the need to disentangle the star-formation and AGN contributions to the total radio emission, for which very long baseline interferometry would offer excellent spatial information to supplement multi-wavelength analysis.

References

- Becker, R.H., White, R.L., Helfand, D.J., 1995, *ApJ*, 450, 559
- Condon, J.J., Cotton, W.D., Fomalont, E.B., Kellermann, K.I., Miller, N., Perley, R.A., Scott, D., Vernstrom, T., & Wall, J.V., 2012, *ApJ*, 758, 23
- Condon, J.J., Kellermann, K.I., Kimball, A.E., Ivezić, Ž., Perley, R.A., 2013, *ApJ*, 768, 37
- Hartley, P., Jackson, N., Sluse, D., Stacey, H.R., & Vives-Arias, H., 2019, *MNRAS*, 485, 3009
- Hwang, Hsiang-Chih, Zakamska, N.L., Alexandroff, R.M., Hamann, F., Greene, J.E., Perrotta, S., Richards, & G.T., 2018, *MNRAS*, 477, 830
- Jarvis, M.J., et al., 2015, *PoS*, arXiv:1412.5753
- Jarvis, M.J., et al., 2016, *PoS*, arXiv:1709.01901
- Jarvis, M.E., Harrison, C.M., Thomson, A.P., Circosta, C., Mainieri, V., Alexander, D.M., Edge, A.C., Lansbury, G.B., Molyneux, S.J. & Mullaney, J.R., 2019, *MNRAS*, 485, 2710
- Kalfountzou, E., Stevens, J.A., Jarvis, M.J., Hardcastle, M.J., Wilner, D., Elvis, M., Page, M.J., Trichas, M., & Smith, D.J.B., 2017, *MNRAS*, 471, 28
- Kimball, A.E., Kellermann, K.I., Condon, J.J., Ivezić, Ž., & Perley, R.A., 2011, *ApJ* (Letters), 739, L29
- Lähteenmäki, A., Järvelä, E., Ramakrishnan, V., Tornikoski, M., Tammi, J., Vera, R.J.C., & Chamani, W., 2018, *A&A* (Letters), 614, L1
- Laor, A. & Behar, E., 2008, *MNRAS*, 390, 847
- Malefahlo, E., Santos, M.G., Jarvis, M.J., White, S.V., & Zwart, J.T.L., 2019, *submitted to MNRAS*, arXiv:1908.05316
- Mancuso, C., Lapi, A., Prandoni, I., Obi, I., Gonzalez-Nuevo, J., Perrotta, F., Bressan, A., Celotti, A., & Danese, L., 2017, *ApJ*, 842, 95
- McAlpine, K., et al., 2015, *PoS*, arXiv:1412.5771
- White, S.V., Jarvis, M.J., Häußler, B., & Maddox, N. 2015, *MNRAS*, 448, 2665
- White, S.V., Jarvis, M.J., Kalfountzou, E., Hardcastle, M.J., Verma, A., Cao Orjales, J.M., & Stevens, J. 2017, *MNRAS*, 468, 217
- Wilman, R.J., Miller, L., Jarvis, M.J., Mauch, T., Levrier, F., Abdalla, F.B., Rawlings, S., Klöckner, H.-R., Obreschkow, D., Olteanu, D., & Young, S., 2008, *MNRAS*, 388, 1335
- Wong, O.I., Koss, M.J., Schawinski, K., Kapińska, A.D., Lamperti, I., Oh, K., Ricci, C., Berney, S., Trakhtenbrot, B., 2016, *MNRAS*, 460, 1588